City Research Online

City, University of London Institutional Repository

Citation: Shuhui, L., Fu, X., Jaithwa, I., Alonso, E., Fairbank, M. & Wunsch, D. C. (2015). Control of Three-Phase Grid-Connected Microgrids Using Artificial Neural Networks. Paper presented at the 7th International Joint Conference on Computational Intelligence (IJCCI 2015), 12-11-2015 - 14-11-2015, Lisbon, Portugal.

This is the accepted version of the paper.

This version of the publication may differ from the final published version.

Permanent repository link: https://openaccess.city.ac.uk/id/eprint/12813/

Link to published version:

Copyright: City Research Online aims to make research outputs of City, University of London available to a wider audience. Copyright and Moral Rights remain with the author(s) and/or copyright holders. URLs from City Research Online may be freely distributed and linked to.

Reuse: Copies of full items can be used for personal research or study, educational, or not-for-profit purposes without prior permission or charge. Provided that the authors, title and full bibliographic details are credited, a hyperlink and/or URL is given for the original metadata page and the content is not changed in any way.

City Research Online: http://openaccess.city.ac.uk/ publications@city.ac.uk

Control of Three-Phase Grid-Connected Microgrids Using Artificial Neural Networks

Shuhui Li[1], Xingang Fu[1], Ishan Jaithwa[1], Eduardo Alonso[2], Michael Fairbank[2] and Donald C. Wunsch[3]

[1]*Department of Electrical and Computer Engineering, The University of Alabama, Tuscaloosa, AL, USA*

[2]*Department of Computer Science, City University London, London, UK*

[3]*Department of Electrical and Computer Engineering, Missouri University of Science and Technology, Rolla, MO, USA*

sli@eng.ua.edu, {xf, ijaithwa}@crimson.ua.edu, E.Alonso@city.ac.uk, michael.fairbank@virgin.net, dwunsch@mst.edu

Keywords: *neural network control, microgrid, distributed energy resources, grid-connected converter*

Abstract: A microgrid consists of a variety of inverter-interfaced distributed energy resources (DERs). A key issue is how to control DERs within the microgrid and how to connect them to or disconnect them from the microgrid quickly. This paper presents a strategy for controlling inverter-interfaced DERs within a microgrid using an artificial neural network, which implements a dynamic programming algorithm and is trained with a new Levenberg-Marquardt backpropagation algorithm. Compared to conventional control methods, our neural network controller exhibits fast response time, low overshoot, and, in general, the best performance. In particular, the neural network controller can quickly connect or disconnect inverter-interfaced DERs without the need for a synchronization controller, efficiently track fast-changing reference commands, tolerate system disturbances, and satisfy control requirements at grid-connected mode, islanding mode, and their transition.

1 INTRODUCTION

Distributed generation (DG) is an approach that employs small-scale technologies to produce electricity close to the end users of power. DG technologies often consist of modular and renewable-energy generators. They offer a number of potential benefits over traditional power generators, such as lower-cost electricity and increased power reliability and security with fewer environmental consequences. A microgrid is defined as an interconnected network of distributed energy systems (loads and DG resources) that can function with or without a connection to the main grid. This new approach to designing and building future smart grids focuses on creating a plan for local energy delivery that meets the needs of the constituents being served. Microgrids can efficiently integrate small-scale DGs into low-voltage (LV) systems and supply the demand of local customers, so their development is expected to yield the following benefits: 1) enable the development of sustainable and green electricity; 2) enable larger public participation in the investment in small-scale generation; 3) reduce the number of marginal central power plants, 4) improve the security of the supply; 5) reduce losses; and 6) enable better network congestion management and control to improve power quality. One important issue in microgrid operation is how to control the inverter-interfaced distributed energy resources (DERs). Conventionally, these DERs are controlled using standard vector control technology (mostly, Proportional Integral, PI, controllers). Within this framework, different solutions for connecting them to and disconnecting them from the main network have been proposed (Blaabjerg et al., 2006). Specifically, implementing a fast and accurate grid voltage synchronization algorithm (Rodríguez et al., 2012) is crucial, though this usually involves a complicated process. Recent studies have shown that an artificial neural network can be trained and used to control a grid-connected converter (Li et al., 2014). In (Li et al.,

2014), the neural network performance was evaluated mainly for d- and q-axis current tracking control of a grid-connected converter in a vector control condition. Compared to conventional vector control methods, the neural network yielded an extremely fast response time, low overshoot, and, in general, the best performance. The purpose of this paper is to investigate neural network control technology for control of grid-connect converters, including PQ and PV converters, and for control of a microgrid containing PQ and PV grid-connected converters. The main contributions of the paper include: 1) a neural network vector control strategy for optimal control of grid-connected converters (GCC); 2) a neural network design and training algorithm that can handle GCC control properly under physical system constraints; 3) control of inverter-interfaced DERs in a microgrid without using a synchronization control technique; and 4) investigation of neural network vector control for a microgrid network.

2 CONTROL ARCHITECTURES

The control objective of a DER is to manage the active power transferred from the dc side to the ac side and to control the reactive power absorbed from the ac grid. This active and reactive power control usually is transformed into d- and q-axis current control (Li et al., 2011). In the d-q reference frame and using the motor sign convention, the voltage balance across the grid filter is:

$$\begin{bmatrix} v_d \\ v_q \end{bmatrix} = R_f \begin{bmatrix} i_d \\ i_q \end{bmatrix} + L_f \frac{d}{dt} \begin{bmatrix} i_d \\ i_q \end{bmatrix} + \omega_s L_f \begin{bmatrix} -i_q \\ i_d \end{bmatrix} + \begin{bmatrix} v_{d1} \\ v_{q1} \end{bmatrix} \quad (1)$$

in which v_d and v_q represent the Point of Common Coupling (PCC) d- and q-axis voltages, i_d and i_q are the d- and q-axis currents from the grid to the DER, ω_s is the angular frequency of the PCC voltage, and $v_{d1}$and v_{q1} are the inverter's d- and q-axis output voltages. L_f and R_f are the inductance and resistance of the grid filter, respectively. Using the PCC voltage-oriented frame (Li et al., 2011; Li et al., 2014), the instant active and reactive powers absorbed by the DER from the grid are proportional to the grid's d- and q-axis currents, respectively, as shown by Eqs. (2) and (3):

$$p(t) = v_d i_d + v_q i_q = v_d i_d \quad (2)$$

$$q(t) = v_q i_d - v_d i_q = -v_d i_q \quad (3)$$

2.1 Conventional Control Structure

The conventional standard vector control method of a DER converter implements a nested-loop structure. The control strategy of the inner current loop is developed by rewriting Eq. (1) as:

$$v_{d1} = \left(R_f i_d + L_f \cdot di_d/dt\right) - \omega_s L_f i_q + v_d \quad (4)$$

$$v_{q1} = \left(R_f i_q + L_f \cdot di_q/dt\right) + \omega_s L_f i_d \quad (5)$$

in which the expressions in parentheses are treated as the state equations between the voltage and current on the d- and q-axis loops, and the remaining expressions are treated as compensation terms (Li et al., 2011; Rocabert et al., 2011). The final control voltages,v_{d1}^* and v_{q1}^*, applied to the DER converter include the d- and q-axis voltages, v_d' and v_q', generated by the current-loop controllers, in addition to the compensation terms, as shown in Eq. (6). Hence, the conventional control configuration of the DER converter intends to regulate i_d and i_q using v_d' and v_q', respectively. However, as indicated in (Li et al., 2011), v_d' is only effective for reactive power, or i_q, control, and v_q' is only effective for active power, or i_d, control. Although the final control voltage applied to the converter contains the compensation terms, those compensation terms are not generated by the PI controllers.

$$v_{d1}^* = v_d' - \omega_s L_f i_q + v_d, \quad v_{q1}^* = v_q' + \omega_s L_f i_d \quad (6)$$

2.2 Neural Network Control Structure

Following (Li et al., 2011), our neural network vector control structure of a DER a d-axis loop is used for active power control and a q-axis loop is used for reactive power, or grid voltage support control. The error signal between the measured and reference active power generates a d-axis current reference to the

neural network through a PI controller, while the error signal between the actual and desired reactive power generates a q-axis current reference. The neural network, known here as the action network, is applied to the DER inverter through a pulse width modulation (PWM) mechanism to regulate the DER output voltage in the three-phase ac system. The ratio of the inverter output voltage to the output of the action network is a gain of k_{PWM}, which equals $V_{dc}/2$ if the amplitude of the triangle voltage waveform in the PWM scheme is 1V (Mohan et al., 2002). The integrated DER system, described by Eq. (1), is rearranged into the standard state-space representation using Eq. (7), in which the system states are i_d and i_q, PCC voltages v_d and v_q normally are constant, and converter output voltages $v_{d1}$and v_{q1} are the control voltages to be specified by the output of the action network. For digital control implementation and offline training of the neural network, the discrete equivalent of the continuous system state-space model, Eq. (7), must be obtained using Eq. (8), in which T_s represents the sampling period, k is an integer time step, **F** is the system matrix, and **G** is the matrix associated with the control voltage. In this paper, a zero-order-hold discrete equivalent (Franklin et al., 1998) is used to convert the continuous state-space model of the system in Eq. (7) to the discrete state-space model in Eq. (8). In all experiments, T_s=1ms.

$$\frac{d}{dt}\begin{bmatrix} i_d \\ i_q \end{bmatrix} = -\begin{bmatrix} R_f/L_f & -\omega_s \\ \omega_s & R_f/L_f \end{bmatrix}\begin{bmatrix} i_d \\ i_q \end{bmatrix} - \frac{1}{L_f}\begin{bmatrix} v_{d1} \\ v_{q1} \end{bmatrix} + \frac{1}{L_f}\begin{bmatrix} v_d \\ v_q \end{bmatrix} \tag{7}$$

$$\begin{bmatrix} i_d(kT_s+T_s) \\ i_q(kT_s+T_s) \end{bmatrix} = \mathbf{F}\begin{bmatrix} i_d(kT_s) \\ i_q(kT_s) \end{bmatrix} + \mathbf{G}\begin{bmatrix} v_{d1}(kT_s)-v_d \\ v_{q1}(kT_s)-v_q \end{bmatrix} \tag{8}$$

The action network is a fully connected multi-layer perceptron (Hagan et al., 2002) with six input nodes, two hidden layers having six nodes each, two output nodes, and shortcut connections between all pairs of layers, with hyperbolic tangent functions at all nodes. These six input components correspond to 1) the d- and q-axis current signals, 2) the two error signals of the d- and q-axis currents, and 3) the two integrals of the error signals. To simplify the expressions, the discrete system model in Eq. (8) is represented by:

$$\vec{i}_{dq}(k+1) = \mathbf{F}\cdot\vec{i}_{dq}(k) + \mathbf{G}\cdot\left(\vec{v}_{dq1}(k) - \vec{v}_{dq}\right) \tag{9}$$

For a reference dq current, the control action applied to the system is expressed by:

$$\vec{v}_{dq1}(k) = k_{PWM}\cdot A\left(\vec{i}_{dq}(k), \vec{i}_{dq}(k) - \vec{i}_{dq_ref}(k), \vec{s}_{dq}(k), \vec{w}\right) \tag{10}$$

in which $\vec{w}$ represents the weight vector of the action network, and $\vec{s}_{dq}(k)$ represents the network's integral input vector defined by $\vec{s}(k) = \int_0^k \left(\vec{i}_{dq}(t) - \vec{i}_{da_ref}(t)\right)dt$. To prevent the neural network controller from being affected by the PCC voltage variation, we used a strategy that introduces the disturbance PCC voltage to the output of the network.

3 NEURAL NETWORK TRAINING

Unlike the conventional standard vector controller, the neural network controller is produced through training using Dynamic Programming (DP). DP employs Bellman's Principle of Optimality (Bellman, 1957) and is a very useful tool for solving optimal control problems (Balakrishnan and Viega, 1996; He et al., 2012). The typical structure of discrete-time DP includes a discrete-time system model and a performance index or cost associated with the system (Wang et al., 2009). The DP cost function associated with the vector-controlled system is defined as:

$$C\left(\overrightarrow{i_{dq}}(j), \vec{w}\right) = \sum_{k=j}^{\infty} \gamma^{k-j} U(\overrightarrow{e_{dq}}(k)), j > 0, 0 < \gamma \le 1 \tag{11}$$

whith γ a discount factor, $\overrightarrow{e_{dq}}(k) = \left(e_d(k), e_q(k)\right)$ $= \left(i_d(k) - i_{d_ref}(k), i_q(k) - i_{q_ref}(k)\right)$ and U is defined as:

$$U(\overrightarrow{e_{dq}}(k)) = \left[e_d^2(k) + e_q^2(k)\right]^{\alpha} = \left\{\left[i_d(k) - i_{d_ref}(k)\right]^2 + \left[i_q(k) - i_{q_ref}(k)\right]^2\right\}^{\alpha}, \alpha > 0 \tag{12}$$

in which α is a constant. The function $C(\cdot)$, depending on the initial time j and the initial state

$\overrightarrow{i_{dq}}(j)$, is referred to as the cost-to-go of state $\overrightarrow{i_{dq}}(j)$ of the DP problem. The objective of the neural network controller is to solve a current tracking problem, i.e., to hold the existing state $\vec{i}_{dq}$ near a given (possibly moving) target state $\vec{i}_{dq}^{*}$ so that the function $C(\cdot)$ in Eq. (11) is minimized. The current-loop action network was trained to minimize the DP cost in Eq. (11) using Levenberg-Marquardt backpropagation (LMBP) (Hagan et al., 2002). LMBP, a variation of Newton's method, minimizes a function that is the sum of squares of a nonlinear function. Using LMBP with a general value for α requires a modification for the cost function $C(\cdot)$ defined in Eq. (11). Consider the cost function $C=\sum_{k=j}^{\infty}\gamma^{k-j}U(\overrightarrow{e_{dq}}(k))$, in which $\gamma=1$, $j=1$, and $k=1,\ldots,N$. Then, C can be written as:

$$C=\sum_{k=1}^{N}U(\overrightarrow{e_{dq}}(k))=\sum_{k=1}^{N}\left(V(k)\right)^{2} \tag{13}$$

in which $V(k)=\sqrt{U(\overrightarrow{e_{dq}}(k))}$ and the gradient $\partial C/\partial\vec{w}$ can be written in matrix form as:

$$\frac{\partial C}{\partial\vec{w}}=\frac{\partial\sum_{k=1}^{N}\left(V(k)\right)^{2}}{\partial\vec{w}}=\sum_{k=1}^{N}2V(k)\frac{\partial V(k)}{\partial\vec{w}}=2J(\vec{w})^{T}\vec{V} \tag{14}$$

in which $\vec{V}=\begin{bmatrix} V(1) & \ldots & V(N)\end{bmatrix}^{T}$, and the Jacobian matrix $J(\vec{w})$ is:

$$J(\vec{w})=\begin{bmatrix}\frac{\partial V(1)}{\partial w_1} & \cdots & \frac{\partial V(1)}{\partial w_M}\\ \vdots & \ddots & \vdots\\ \frac{\partial V(N)}{\partial w_1} & \cdots & \frac{\partial V(N)}{\partial w_M}\end{bmatrix} \tag{15}$$

Therefore, the process of updating the weights using LMBP for a neural network controller can be expressed as:

$$\Delta\vec{w}=-\left[J(\vec{w})^{T}J(\vec{w})+\mu\mathbf{I}\right]^{-1}J(\vec{w})^{T}\vec{V} \tag{16}$$

The parameter μ was dynamically adjusted to ensure that the training followed the decreasing direction of the cost function. When μ increased, (16) approached the steepest descent algorithm with a small learning rate, while as μ decreased, the algorithm (16) approached Gauss-Newton, which typically provides faster convergence. In order to increase the speed of computation, the weight update in Eq. (16) was conducted using Cholesky factorization, which is roughly twice as efficient as lower-upper decomposition for solving systems of linear equations (Press et al., 1992).

To train the action network, the system data associated with Eq. (7) had to be specified. The training procedure for the current-loop action network involved: 1) randomly generating a sample initial state $i_{dq}(j)$; 2) randomly generating a changing sample reference dq current time sequence; 3) unrolling the trajectory of the system from the initial state; 4) training the current-loop neural network based on Eq. (16); and 5) repeating the process for all of the sample initial states and reference dq currents until reaching a stop criterion associated with the DP cost. All of the network weights initially were randomized using a uniform distribution with zero mean and 0.1 variance.The generation of the reference current considered the physical constraints of a practical DER inverter system. The randomly generated d- and q-axis reference currents first were chosen uniformly from [$-I_{rated}$,I_{rated}], in which I_{rated} represents the rated inverter line current. Then, these randomly generated d- and q-axis current values were checked and modified to ensure that their resultant magnitude did not exceed the inverter's rated current limit and/or the control voltage did not exceed the converter's PWM saturation limit. From the neural network standpoint, the PWM saturation constraint indicates the maximum positive or negative voltage that the action network can output. Therefore, if a reference dq current requires a control voltage that exceeds the acceptable voltage range of the action network, it is impossible to reduce the cost during the training of the action network. The neural network controller is trained offline, and no training occurs in the real-time control stage. Without online training, a real-time control action can be computed very quickly using modern DSP chips. The most

important issue is the sampling time. However, an optimal neural network controller can be trained using a large sampling time based on the DP principle, while tuning a conventional controller for the same sampling time could be very difficult or impossible. Therefore, the neural network controller actually has lesser sampling and computing power requirements during the real-time control process.

4 CONTROL OF INVERTER DER

The key requirements for controlling inverter-interfaced DERs within a microgrid include: 1) active power control; 2) reactive power control; 3) grid voltage support control, and 4) control under physical constraints. If a GCC can meet these control requirements, it can be applied broadly to power and energy system applications involving GCCs. In our experiments, the system data and controller parameters for various control purposes are as in Tables 1 and 2:

Table 1: Systems data.

Component	Parameter	Value
AC system	Line voltage	400V
	Frequency	60Hz
Transmission line	Resistance	0.0076Ω
	Inductance	0.154mH
Grid-filter	Resistance	0.006Ω
	Inductance	1mH
DER converter	Switching frequency	3000Hz
DC system	Voltage	700V

Table 2: Parameters of DER controller (k_p – proportional gain, k_i – integral gain).

Approach	Controller	Gain (k_p / k_i)
Conventional	Current loop	1.54 / 53.52
	AC bus voltage	1.09 / 35.6
Neural network	Current loop	Neural network
	AC bus voltage	1.09 / 35.6

The PCC bus was connected to the microgrid through a transmission line that was modeled by an impedance. A fault-load was connected before the PCC bus to evaluate how the controller behaves when a fault appears in the grid. The DER inverter's switching frequency was 3kHz. Typical strategies for operating a DER in a microgrid include PQ-inverter DER and PV-inverter DER (Katiraei et al., 2008). In the power converter switching condition, the controller can be evaluated under close to real-life conditions. The position of the PCC voltage space vector θ_v was obtained directly from the PCC voltage measurement in the α-β reference frame given by:

$$\theta_v = \tan^{-1}\left(v_\alpha / v_\beta\right) \tag{17}$$

4.1 Control of PQ-Inverter DERs

A PQ-inverter DER operates by injecting active and reactive power into the microgrid. The active and reactive power control at the PCC of an inverter-interfaced DER is converted to d- and q-axis current control. The d- and q-axis current references, i_d^* and i_q^*, are obtained either through a PI control mechanism or by calculating Eqs. (2) and (3), as discussed in (Li et al., 2011):

$$i_d^* = P_{ac}^* / v_d\,, \qquad i_q^* = -Q_{ac}^* / v_d \tag{18}$$

The desired active power of the DER normally is generated according to either a maximum power capture rule for a renewable DER unit or an active power control demand from the microgrid central control (MGCC) level. The desired reactive power is issued either locally for the unity power factor or centrally according to a control command from the MGCC.

Fig. 1 in the Appendix presents a case study of the PQ-controlled DER using the conventional and neural network control methods. At first, the active and reactive power references were 40kW and 0kVar, respectively. After the system started, the neural network controller quickly regulated the active and reactive power of the DER to the reference values. When the reference power took on new values of -50kW/20kVar and -100kW/10kVar at t=2sec and t=4sec, respectively, the neural network controller immediately restored DER power to the new reference values (Fig. 1a). As shown in Fig. 1c, the three-phase

grid current was properly balanced. For any other commanded change of the reference power within the DER-rated power limit, the system could be adjusted immediately to the new reference power, demonstrating the strong optimal control capability of the neural network vector controller. Compared to the neural network controller, the conventional controller was slower, had a higher oscillation, and took longer to reach its target value. This was more evident at t=0sec when starting the system.

4.2 Control of PV-Inverter DERs

One critical disadvantage of the PQ-inverter DER is that the PCC bus voltage changes as active and reactive power are transferred through the PCC and as the load varies. A PV-inverter DER operates by injecting active power into the microgrid while simultaneously maintaining the PCC bus voltage at a desired value. The desired active power is formed in the same way as that used in a PQ-inverter DER, but the reactive power is controlled according to the error signal between the desired and the actual PCC bus voltage to which the inverter is connected. Therefore, as the PCC bus voltage fluctuates, so does the reference q-axis current generated by a PI controller.

Fig. 2 in Appendix presents a case study of the PV-inverter DER using the conventional and neural network controllers. The active power reference was the same as that used in the case study presented in Fig. 1, while the reference PCC voltage was 1pu. After the system started, the neural network controller quickly regulated the active power of the DER and the PCC bus voltage to the reference values. The inverter initially absorbed active power from the grid, and the reactive power was generated so as to maintain the PCC voltage at 1pu. When the reference active power in the ac system began to generate at t=2sec, the reactive power shifted from generating to absorbing. At t=4sec, the reactive power absorbed more in order to maintain the PCC voltage for the increased active power generated by the DER (Fig. 2a). Similar to Fig. 1, this case study demonstrates the excellent performance of the neural network vector controller for the PV-inverter DER. However, using the conventional controller, a large oscillation occurred each time the DER active power changed significantly (Fig. 2b).

4.3 Control of DER Inverter under Constraints

In practice, a DER inverter cannot operate beyond the rated power and PWM saturation of the converter. To handle DER operation under such conditions, we propose controlling the DER by maintaining the effectiveness of the active power control while meeting the reactive power control demand as much as possible. This is expressed as: minimize $\left|Q_{ac} - Q_{ac}^{*}\right|$, subject to

$$\begin{cases} P_{ac} = P_{ac}^{*} \\ \sqrt{i_d^2 + i_q^2} \le I_{rated}, \quad \sqrt{\dfrac{v_{d1}^2 + v_{q1}^2}{3}} \le \dfrac{V_{dc}}{2\sqrt{2}} \end{cases} .$$

For the conventional controller, the following strategies are used. To prevent the DER converter from exceeding the PWM saturation limit, Eq. (19) is applied if the amplitude of the reference voltage generated by the inner current-loop controller exceeds the converter's PWM saturation limit (Gagnon, 2009; Li et al., 2011), in which $v_{d1_new}^{*}$ and $v_{q1_new}^{*}$ are the d and q components of the modified controller output voltage, and $V_{max}$is the maximum allowable dq voltage:

$$v_{d1_new}^{*} = V_{\max}\cos\left(\angle v_{dq1}^{*}\right) \quad v_{q1_new}^{*} = V_{\max}\sin\left(\angle v_{dq1}^{*}\right) \tag{19}$$

To prevent the DER converter from exceeding the rated current, Eq. (20) is employed if the amplitude of the reference current generated by the outer control loop exceeds the rated current limit, i.e., the d-axis current reference i_d^{*} is kept constant to maintain active power control effectiveness, while the q-axis current reference i_q^{*} is modified to satisfy the reactive power or ac system bus voltage support control demand as much as possible (Gagnon, 2009; Li et al., 2011):

$$i_{d_new}^{*} = i_d^{*} \quad i_{q_new}^{*} = \text{sign}\ \left(i_q^{*}\right)\cdot\sqrt{\left(i_{dq_\max}^{*}\right)^2 - \left(i_d^{*}\right)^2} \tag{20}$$

For the neural network controller, if $|i_{dq}^*|$ generated by the dc-voltage or the active and reactive power control loops exceeds the rated current limit, i_d^* and i_q^* are modified by Eq. (20) before being applied to the action network (Li et al., 2011); if $|v_{dq1}^*|$ generated by the current control loops exceeds the PWM saturation limit, the action neural network automatically turns into a state by regulating v_{q1} to maintain the effectiveness of the active power control while restraining v_{d1} to meet the reactive power control demand as much as possible.

Fig. 3 in the Appendix presents a case study of the PQ-inverter DER in which there was high demand for reactive power generation. The active power reference was the same as that used in the case study illustrated in Fig. 2, while the reactive power demand caused the required control voltage to exceed the inverter's PWM saturation limit at t=3sec. As Fig. 3a illustrates, the neural network controller automatically restrained the reactive power control while maintaining the effectiveness of the active power control at t=3sec. At t=5sec, when the reactive power demand generation decreased, causing the control voltage to fall below the PWM saturation limit, the neural network controller returned to its normal control condition immediately. For the conventional controller, however, when the control voltage exceeded the inverter's PWM saturation limit at t=3sec, the system could not follow the control commands properly due to its competing control nature (Li et al., 2011), as shown in Fig. 3b.

Fig. 4 in the Appendix presents a case study of the PV-inverter DER for PCC voltage support control under a moderate voltage drop caused by a fault at t=3sec. Due to the inverter's PWM saturation constraint, the neural network controller could not maintain the PCC voltage at 1pu to compensate for the voltage drop (Fig. 4c). Instead, it operated by maintaining the effectiveness of the active power control while providing PCC voltage support control as much as possible. At t=5sec, when the short circuit was cleared, the neural network controller returned to its normal operating condition, and the PCC bus voltage recovered to the rated bus voltage quickly, thus demonstrating the neural network controller's excellent PCC voltage support control under the physical constraints of DERs. For the conventional controller, however, when the required control voltage exceeded the inverter's PWM saturation limit shortly after t=3sec, the system could not follow the control commands properly, as shown in Fig. 4b and 4d.

5 MICROGRID CONTROL AND STABILITY ANALYSIS

5.1 A Benchmark Microgrid Network

A typical benchmark low-voltage (LV) microgrid network was built using MatLab SimPowerSystems and an Opal-RT real-time simulation system, as shown in Fig. 5. The microgrid was supplied through a LV feeder to serve a suburban residential area with a limited number of consumers connected along its length. The microgrid consisted of DGs from the most relevant technologies, such as solar photovoltaics, wind turbines, microturbines, and fuel cells. The impedance data for various line types used in the network, as well as detailed information about the installed capacities of the microturbine, fuel cell, and battery storage device, are available in (Papathanassiou et al., 2005)). The loads were assumed to have similar load patterns. The power factor was 0.85 lagging. The DGs were connected to the following buses: solar on buses 6 and 7, wind on bus 6, microturbine on bus 5, fuel cell on bus 8, and battery on bus 4. Thus, the benchmark network maintained the important technical characteristics of real-life utility distribution systems, while dispensing with the complexity of actual networks, to permit the efficient modeling and simulation of the microgrid's operation.

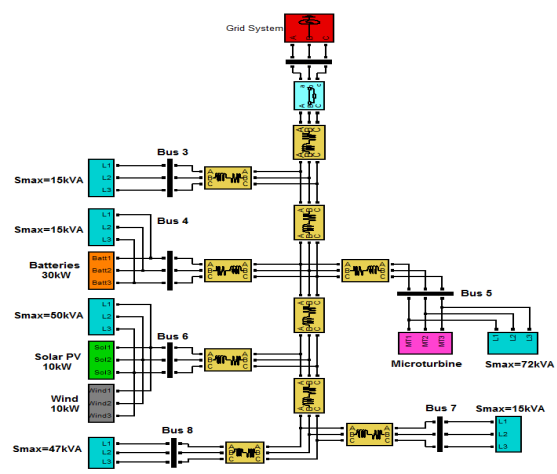

Figure 5. Benchmark LV microgrid networks using neural controllers.

5.2 DER Synchronization

Before connecting any DER to the microgrid, it must be synchronized accurately with the network voltage to avoid over currents (Rodríguez et al., 2012). Most grid-tied systems use a phase locked loop (PLL) for synchronization (Rodríguez et al., 2012). Many grid synchronization applications for three-phase systems are based on the implementation of synchronous reference frame PLLs (SRF-PLL) (Chung, 2000), in which the three-phase grid voltage is transformed using Clarke and Park transformation into a stationary reference frame (Chung, 2000). The quadrature component of the voltage resulting from this synchronous transformation, namely, v_q, is conducted to zero using a PI controller. The output of the PI controller provides the estimated value of the rotating frequency of the SRF-PLL. Integrating this frequency yields the phase angle of the SRF (θ). When the quadrature component, v_q, is equal to zero, θ matches the phase angle of the input voltage vector; hence, the PLL is synchronized with the positive-sequence component of the grid. Although the SRF-PLL performs appropriately under balanced voltages, it exhibits highly deficient performance under unbalanced and distorted grid conditions (Rocabert et al., 2011)). Moreover, its performance is very sensitive to sudden changes in the phase angle, which makes it less reliable when synchronizing power converters with the grid (Rocabert et al., 2011). However, this is not the case when using the neural network vector controller. The neural controller can better satisfy the requirements of an ideal controller with its close to zero rise time, zero overshoot, and zero settling time. Therefore, it is possible to connect the inverter-interfaced DERs to the grid using the neural vector controller directly, without pre-synchronization.

Fig. 6 in Appendix compares the performance of the conventional and neural network control methods without synchronization control when connecting the two-DER systems to the grid. Neither DER was connected to the MG before t=1sec. When DER1 and DER2 were connected to the MG at 1sec and 2sec, respectively, the system reached the reference current or power demand of each micro-source almost immediately, without any over current, using the neural network controller. However, using the conventional controller, a large oscillation appeared in the ac system three-phase currents, depending on the extent to which the DER was synchronized with the grid when closing the switch. The comparison demonstrates the superior synchronization capability of the neural network vector controller, which is due to this controller having been trained to implement the optimal control according to the DP principle. An ideal optimal controller would allow a reference value to be reached immediately without any oscillation. A well-trained neural network controller based on the DP principle could exhibit very close to ideal performance to satisfy the need for fast synchronization.

5.3 Microgrid Control and Stability

The performance of neural networks for microgrid control was further evaluated under the following conditions. Initially, the microgrid was connected to the main grid. The solar and wind turbine at Bus 6 operated in the maximum power extraction and PCC voltage control mode. The PCC voltage control has the advantage of providing a better voltage quality to the microgrid, which is particularly important under the microgrid islanding condition. The converter of the microturbine at Bus 5 operated in the V-f control mode based on the conventional droop control concept (Bottrell et al., 2013; Lee et al., 2013; Rowe et al., 2013), which is a necessary requirement especially in the microgrid islanding operating condition. The droop control is implemented by

$$f_s = f_{s0} - r_f\left(P_{ac} - P_{ac0}\right), V_{ac} = V_{ac0} - r_V\left(Q_{ac} - Q_{ac0}\right) \qquad (21)$$

where f_{s0} and V_{ac0} represent the nominal frequency and voltage, P_{ac0} and Q_{ac0} signify the PCC active and reactive power that the microturbine is expected to generate at the nominal frequency and voltage, r_f and r_V are the coefficients corresponding to frequency- and voltage-droop characteristics, and f_s, V_{ac}, and P_{ac} and Q_{ac} represent the instant frequency, voltage, and PCC active and reactive powers, respectively. The battery at Bus 4 employed the vector control structure with the d-axis loop for active power control and q-axis loop for PCC voltage control. Again, with the PCC voltage control, a better voltage quality across the microgrid can be achieved. The reference active power command P^*_{ac} of the battery converter is generated based on the frequency-droop characteristic as shown by

$$P_{ac}^{*} = P_{ac0}^{*} - \frac{1}{R_f}\left(f_s - f_{s0}\right) \tag{22}$$

where P^{*}_{ac0} represents the secondary active reference power command generated by the MGCC. Hence, if the frequency f_s of the microgrid equals to the nominal frequency f_{s0}, the reference power command P^{*}_{ac} of the battery equals to the power command P^{*}_{ac0} from the MGCC; if the frequency f_s of the microgrid is different from the nominal frequency f_{s0}, the reference power command equals to the power command P^{*}_{ac0} from the MGCC plus an adjustment generated according to the droop principle.

Fig. 7 shows the performance of the microgrid in the grid-connected mode, islanding mode, and transition from the grid-tied to islanding mode. Due to variable weather conditions, the power transferred from a wind turbine or solar array changed constantly. This is represented by a changing d-axis current as shown in Figs. 7a and 7b. Before t=2sec, only wind and solar DERs at Bus 6 were connected to the microgrid. At t=2sec, the battery at Bus 4was connected to the microgrid with full charging power, which increased the power supplied by the grid to the microgrid (Fig. 7e). At t=4sec, non-critical loads within the microgrid were curtailed to prepare for the islanding operation, which increased voltage distortion within the microgrid network as demonstrated by higher d- and q-axis current oscillation from wind, solar, and battery DERs in Figs. 7a to 7c. At t=6sec, the battery shifted from charge mode to discharge mode, which decreased the power supplied by the grid even more (Fig. 7e). During the grid-connected mode, the microgrid frequency was stable (Fig. 7d) so that the reference power of the battery converter depended mainly on the charge or discharge power command from the MGCC (Fig. 7c). At t=8sec, the microgrid shifted from the grid-tied mode to the islanding mode. Therefore, no power was transferred from the grid to the microgrid after t=8sec (Fig. 7e) and at the same time there was a large increase of the power supplied by the microturbine (Fig. 7f). Note that in Figs. 7e and 7f, the motor sign convention is used to represent the power absorbed by the microgrid from the grid or power absorbed by the microturbine from the distribution network. In the islanding mode, the microgrid frequency was more sensitive to the load and DER power variations (Fig. 7d). The frequency alteration caused the battery controller to adjust the MGCC power reference according to the droop principle (Eq. (22) and Fig. 7c). During both the grid-tied and islanding modes, the microgrid voltage was properly maintained around the desired value (Figs. 7g and 7h). Although there was a high oscillation in DER currents during the transition from the grid-tied to islanding mode (Fig. 7i), the current oscillation of the loads within the microgrid is not obvious (Fig. 7j).

For each DER, only information about the nominal PCC voltage, nominal dc voltage, and resistance and inductance values of the grid filter is required to train the neural network controller of the DER converter. The same information is needed for the design of a conventional controller, as well. After the training, the neural network controller can be applied to the DER converters in a microgrid, although the distribution system structure seen by each DER may be different. Again, the study shown by Fig. 7 demonstrates a great performance and stability of the microgrid in grid-tied mode, islanding mode, and transition from the grid-tied to islanding mode by using the proposed neural network vector controllers, which is an important issue in microgrid operation (Bottrell et al., 2013; Lee et al., 2013; Rowe et al., 2013).

6 CONCLUSIONS

This paper presented a neural network control mechanism for the control of a microgrid and the distributed energy sources within the microgrid. This controller, which implements dynamic programming, was trained with a Levenberg-Marquardt backpropagation algorithm. Compared to conventional vector control methods, the neural network controller demonstrated a stronger ability to determine optimal control actions from multiple inputs. It boasts very fast response and close to ideal controller performance. It does not require synchronization to initially connect a DER or a microgrdi to the grid, making it a potential solution to many challenges in the operation and management of DERs and future smart microgrids. Using a neural network control technique, a microgrid can achieve a better voltage profile, high power quality and quick connection or disconnection of a distributed energy source to the microgrid. In future work, we plan to build a micro-scale microgrid system and obtain real data and more solid experiment results.

REFERENCES

S. N. Balakrishnan and V. Biega, Adaptive-critic-based neural networks for aircraft optimal control, *J. Guidance, Control, and Dynamics*, 19: 4, pp. 893–898, 1996.

R. E. Bellman, *Dynamic Programming.* Princeton, NJ: Princeton Univ. Press, 1957.

F. Blaabjerg, R. Teodorescu, M. Liserre, and A. V. Timbus, Overview of control and grid synchronization for distributed power generation systems, *IEEE Trans. Ind. Electron*., 53: 5, pp. 1398–1409, 2006.

N. Bottrell, M. Prodanovic, and T. C. Green, Dynamic stability of a microgrid with an active load, *IEEE Trans. Power Electron*., 28: 11, pp. 5107-5119, 2013.

S.-K. Chung, A phase tracking system for three phase utility interface inverters, *IEEE Trans. Power Electron*., 15: 3, pp. 431–438, 2000.

G. F. Franklin, J. D. Powell, M. L. Workman, *Digital Control of Dynamic Systems*, Addison-Wesley, 1998.

R. Gagnon, Detailed Model of a Doubly-Fed Induction Generator (DFIG) Driven by a Wind Turbine,*The MathWork*, 2009.

M. T. Hagan, H. B. Demuth, and M. H. Beale, *Neural Network Design*, Boston: PWS, 2002.

H. He, N. Zhen, and F. Jian, A three-network architecture for on-line learning and optimization based on adaptive dynamic programming, *Neurocomputing*, 78: 1, pp. 3-13, 2012.

F. Katiraei, R. Iravani, N. Hatziargyriou, and A. Dimeas, Microgrid management, *IEEE Power and Energy Magazine*, 6: 3, 2008, pp. 54-65.

C. Lee, C. Chu, and P. Cheng, A new droop control method for the autonomous operation of distributed energy resource interface converters, *IEEE Trans. Power Electron*., 28: 4, pp. 1980-1993, 2013.

S. Li, M. Fairbank, C. Johnson, D. C. Wunsch and E. Alonso, Artificial neural networks for control of a grid-connected rectifier/inverter under disturbance, dynamic and power converter switching conditions, *IEEE Trans. on NeuralNet. and Learning Systems*, 25: 4, pp. 738–750, 2014.

S. Li, T.A. Haskew, Y. Hong, and L. Xu, Direct-current vector control of three-phase grid-connected rectifier-inverter, *Electric Power System Research,* 81: 2, 2011, pp. 357-366.

N. Mohan, T. M. Undeland, and W. P. Robbins, *Power Electronics: Converters, Applications, and Design*, 3rd ed., John Wiley & Sons Inc., 2002.

S. Papathanassiou, N. Hatziargyriou, and K. Strunz, A benchmark low voltage microgrid network, *Proc. of CIGRE Symposium: Power Systems with Dispersed Generation*, April 2005, Athens, Greece.

W. H. Press, B. P. Flannery, S. A. Teukolsky, and W. T. Vetterling, *Numerical recipes in C: The art of scientific computing* (second edition), Cambridge University Press, 1992, pp. 994.

J. Rocabert, G. M. S. Azevedo, A. Luna, J. M. Guerrero, J. I. Candela, and P. Rodríguez, Intelligent connection agent for three-phase grid-connected microgrids, *IEEE Trans. on Power Electronics*, 26: 10, 2011, pp. 2993-3005.

P. Rodríguez, A. Luna, R. S. Muñoz-Aguilar, I. Etxeberria-Otadui, R. Teodorescu, and F. Blaabjerg, A stationary reference frame grid synchronization system for three-phase grid-connected power converters under adverse grid conditions, *IEEE Trans. Power Electron.*, 27: 1, pp. 99–112, 2012.

C. N. Rowe, T. J. Summers, R. E. Betz, D. J. Cornforth, and T. G. Moore, Arctan power–frequency droop for improved microgrid stability, *IEEE Trans. Power Electron*., 28: 8, pp. 3747-3759, 2013.

F. Y. Wang, H. Zhang, and D. Liu, Adaptive dynamic programming: An introduction, *IEEE Comput. Intell. Mag.*, pp. 39–47, 2009.

APPENDIX

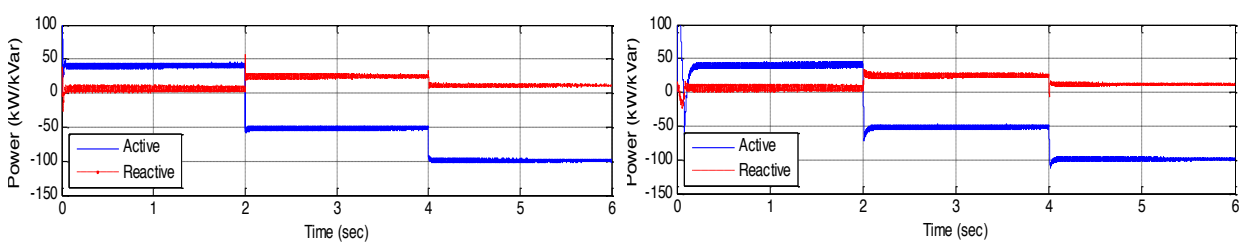

a) Active and reactive power (neural network)

b) Active and reactive power (conventional)

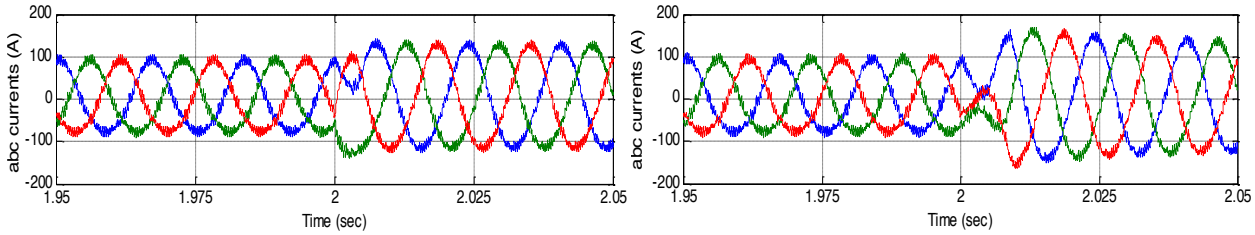

c) Three-phase current (neural network)

d) Three-phase current (conventional)

Fig. 1. Performance of PQ-inverter DER using conventional and neural network controllers (T_s=1ms).

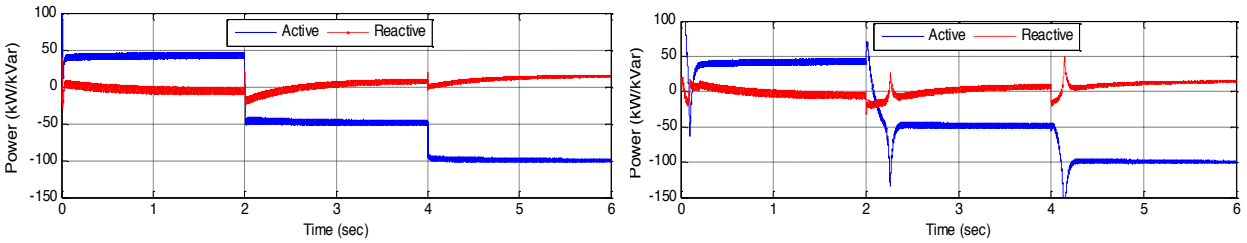

a) Active and reactive power (neural network)

b) Active and reactive power (conventional)

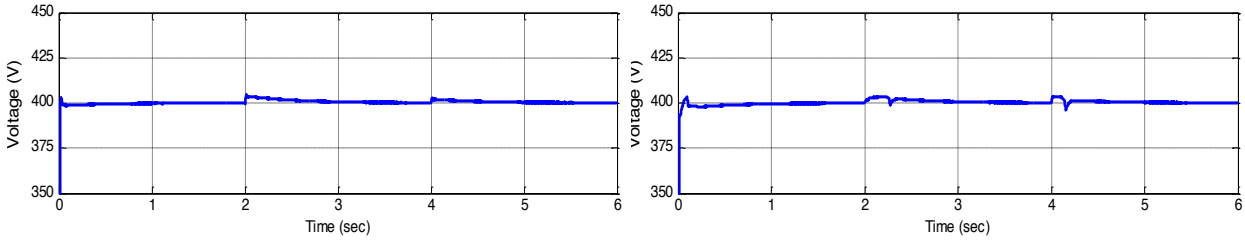

c) PCC voltage (neural network)

d) PCC voltage (conventional)

Fig. 2. Performance of PV-inverter DER using conventional and neural network controllers (T_s=1ms).

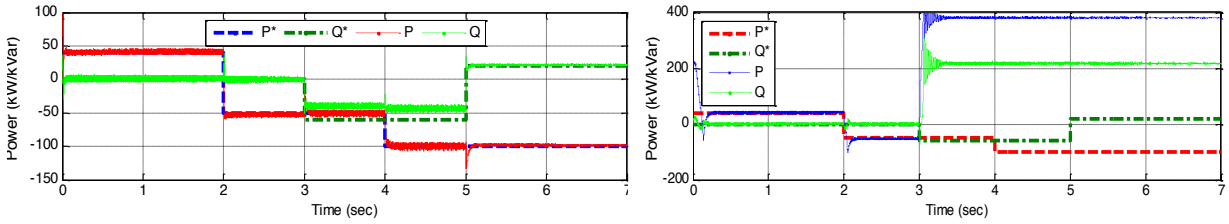

a) Active and reactive power (neural network)

b) Active and reactive power (conventional)

Fig. 3. PQ-inverter DER with constraints using conventional and neural network controllers.

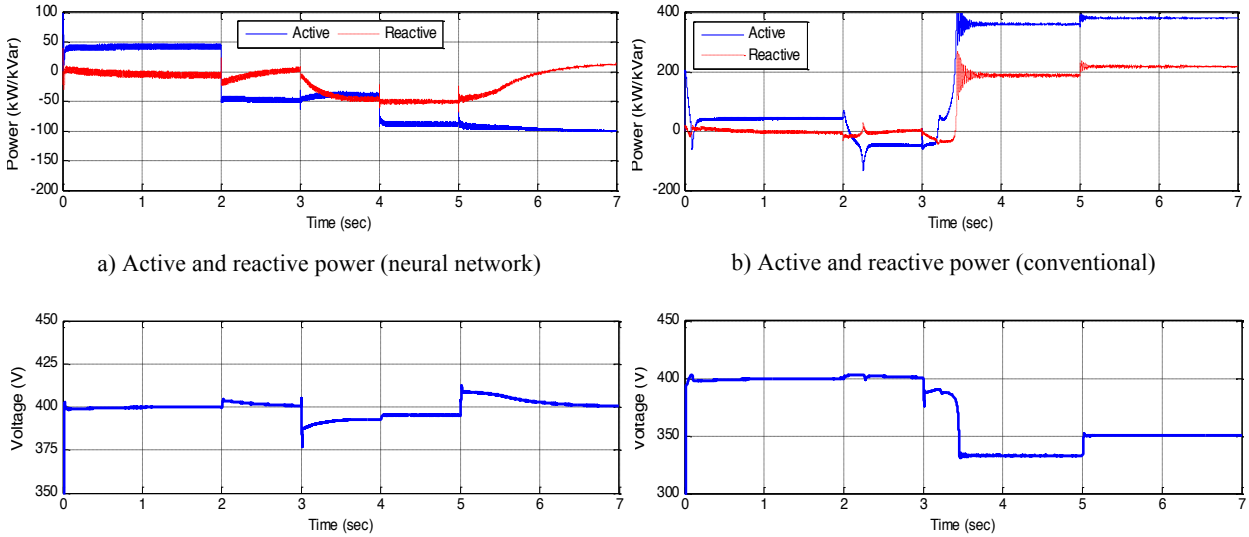

a) Active and reactive power (neural network)

b) Active and reactive power (conventional)

c) PCC voltage (neural network)

d) PCC voltage (conventional)

Fig. 4. PV-inverter with constraints using conventional and neural network controllers.

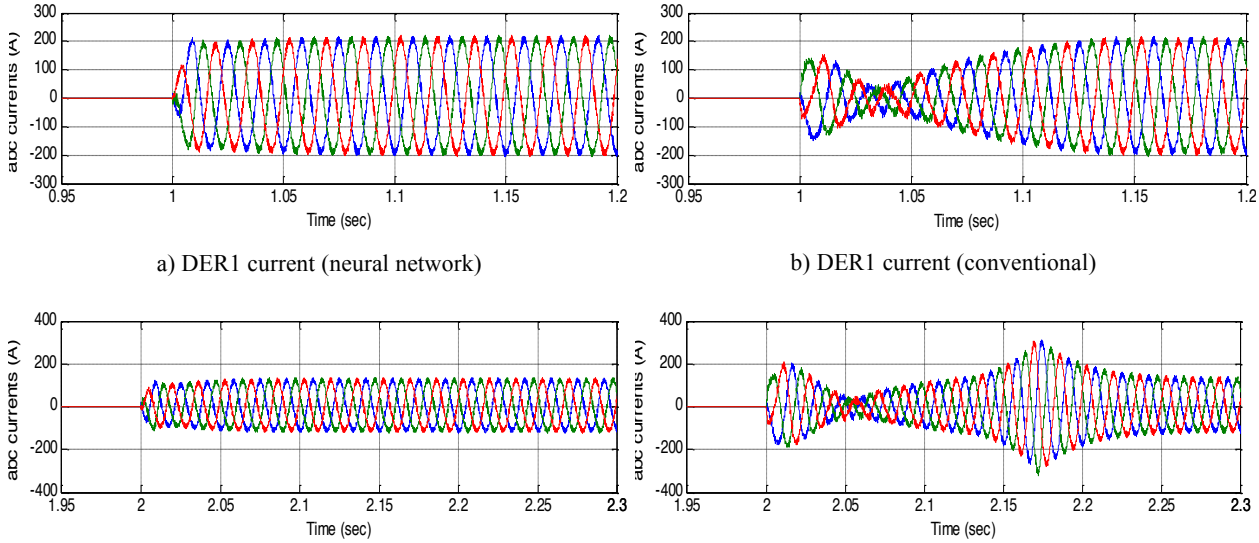

a) DER1 current (neural network)

b) DER1 current (conventional)

c) DER2 current (neural network)

d) DER2 current (conventional)

Fig. 6. Three-phase currents when connecting DERs to the grid without synchronization control.

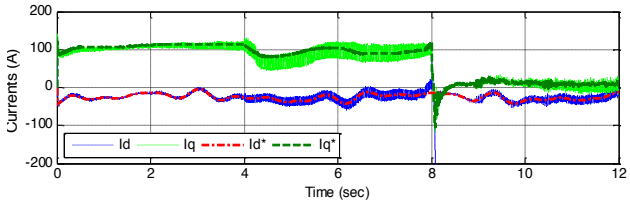

a) Solar inverter d- and q-axis currents

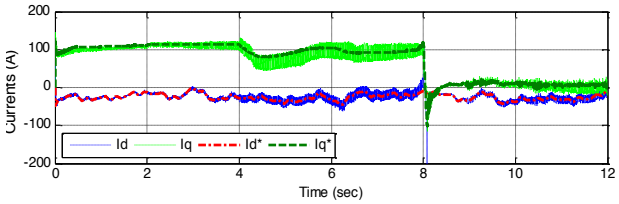

b) Wind turbine inverter d- and q-axis currents

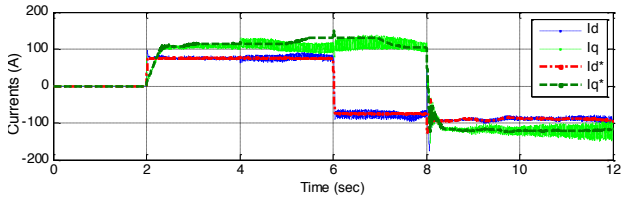

c) Battery inverter d- and q-axis currents

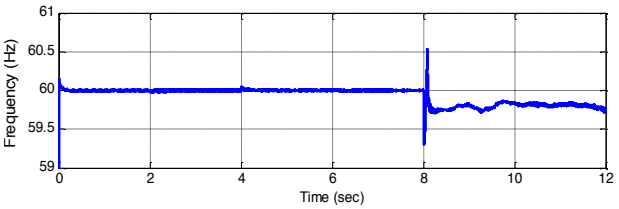

d) Microgrid frequency

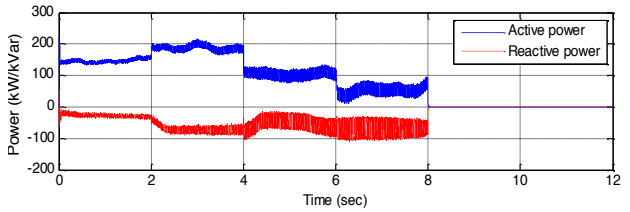

e) Active and reactive power absorbed from the grid

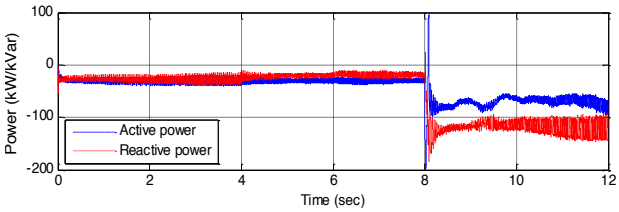

f) Active and reactive power of the microturbine

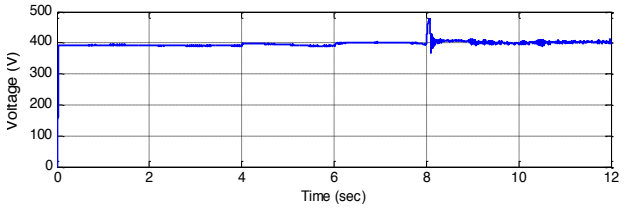

g) RMS line voltage at Bus 4

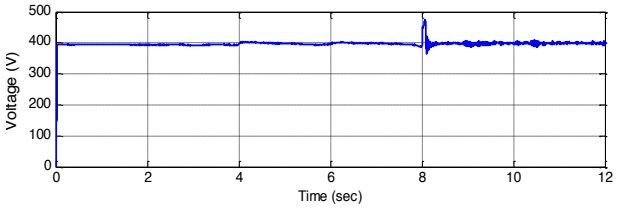

h) RMS line voltage at Bus 6

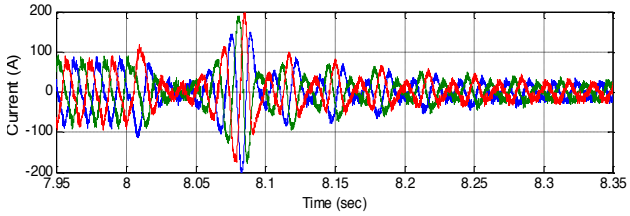

i) Three-phase PCC current of wind DER

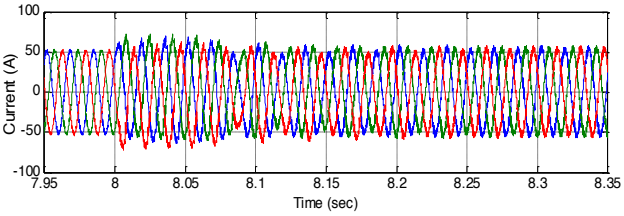

j) Three-phase load current at Bus 8

Fig. 7. Performance of neural network controlled microgrid.